Modulating metal-centered dimerization of a lanthanide chaperone protein for separation of light lanthanides

Wyatt B. Larrinaga, ^{1,3} Jonathan J. Jung, ^{1,3} Chi-Yun Lin, ¹ Amie K. Boal, ^{1,2,*} and Joseph A. Cotruvo, Jr. ^{1,*}

Elucidating details of biology's selective uptake and trafficking of rare earth elements, particularly the lanthanides, has the potential to inspire sustainable biomolecular separations of these essential metals for myriad modern technologies. Here we biochemically and structurally characterize Methylobacterium (Methylorubrum) extorquens LanD, a periplasmic protein from a bacterial gene cluster for lanthanide uptake. This protein provides only four ligands at its surface-exposed lanthanide-binding site, allowing for metal-centered protein dimerization that favors the largest lanthanide, La^{III}. However, the monomer prefers Nd^{III} and Sm^{III}, which are disfavored lanthanides for cellular utilization. Structure-guided mutagenesis of a metal ligand and an outer-sphere residue weakens metal binding to the LanD monomer and enhances dimerization for Pr^{III} and Nd^{III} by 100fold. Selective dimerization enriches high-value Pr^{III} and Nd^{III} relative to low-value La^{III} and Ce^{III} in an all-aqueous process, achieving higher separation factors than lanmodulins, and comparable or better separation factors than common industrial extractants. Finally, we show that LanD interacts with lanmodulin (LanM), a previously characterized periplasmic protein that shares LanD's preference for Nd^{III} and Sm^{III}. Our results suggest that LanD's unusual metal-binding site transfers less-desirable lanthanides to LanM to siphon them away from the pathway for cytosolic import. The properties of LanD show how relatively weak chelators can achieve high selectivity, and they form the basis for the design of protein dimers for separation of adjacent lanthanide pairs and other metal ions.

Significance: Ligand design to effectively discriminate between, and thereby separate, adjacent lanthanide(III) ions is a long-standing challenge. In this work, biochemical studies and X-ray structures reveal how a protein involved in lanthanide uptake binds lanthanide ions, and they suggest that it may help ensure the selective cytosolic import of only the largest lanthanides by siphoning off other lanthanides in the periplasm of lanthanide-utilizing bacteria. Engineering this protein's molecular interface yields separation factors among light lanthanides (lanthanum, cerium, praseodymium, and neodymium) that are comparable to industrial extractants, demonstrating the utility of metal-centered protein dimerization to facilitate difficult separations under mild, aqueous conditions.

Keywords: Metal homeostasis, lanthanide biochemistry, separation science, lanthanome

¹Department of Chemistry, The Pennsylvania State University; University Park, Pennsylvania 16802, United States

²Department of Biochemistry and Molecular Biology, The Pennsylvania State University; University Park, Pennsylvania 16802, United States

³These authors contributed equally to this work.

^{*}Corresponding authors. Email: <u>juc96@psu.edu</u>, <u>akb20@psu.edu</u>

INTRODUCTION

Owing to the, on average, ~0.01 Å difference in ionic radius between adjacent lanthanides, rare earth (RE) separations are challenging but critically important for the clean-energy economy (1). Standard industrial ligands have separation factors (SFs) for adjacent lanthanide (Ln^{III}) ions as low as 1.1 (2, 3). It is also important that ligands disfavor binding of the largest REs, La^{III} and Ce^{III}, as these elements can comprise >70% of many feedstocks (4) but have little value, whereas slightly smaller Pr^{III} and Nd^{III} are substantially more desirable (5). Much recent work has been devoted to creative approaches to improve RE separations. Synthetic molecular approaches to amplify SFs include using rigid, pre-organized ligands to impart higher selectivity over part of the series (6, 7); tug-of-war involving ligands with opposite selectivity trends (8, 9); ligands with unusual selectivity trends (10, 11); and reactivity-based separations (12, 13). Several of these ligands have promising SFs but may bind very tightly or exhibit slow equilibration kinetics (14), both of which may be sub-optimal given the need for multiple adsorption/desorption stages.

Another approach uses dimerizing synthetic ligand:RE complexes (15, 16). Biology has also landed on a similar concept. Although the archetypal highly selective lanthanide-binding protein, lanmodulin (LanM), from *Methylobacterium* (*Methylorubrum*) *extorquens* (*Mex*-LanM) is purely monomeric (17, 18), a LanM from another organism, *Hans*-LanM, dimerizes in a manner sensitive to the ionic radius of the RE (19). This sensitivity likely results from a carboxylate shift that affects coordination number at a metal-binding site in one monomer that connects to the other monomer via a hydrogen-bonding network across an extensive dimer interface (19). However, the SFs of dimerizing small-molecule (15) and natural (19) and engineered (20, 21) protein-based systems, as well as in monomeric LanMs due to their multiple metal sites (17, 22, 23), are dampened by formation of mixed-metal complexes. Therefore, greater radius sensitivity, and thus higher SFs, might be better achieved by a single, interfacial metal site.

Shortly after reporting LanM, our group identified a 6.8-kDa periplasmic protein of unknown function in *M. extorquens*, META1p1781 (LanD, which we now name "landiscernin," for <u>lan</u>thanide-<u>discerning</u> protein), as part of the *lanM* gene cluster that included machinery for lanthanide uptake (*SI Appendix*, **Fig. S1**) (24, 25). The *lanD* gene partially overlaps with the gene encoding the cytosolic component of the ATP-binding cassette (ABC) transporter for import of lanthanides to the cytosol, suggesting a potential role for LanD as a chaperone or accessory protein. Supporting this hypothesis, preliminary studies showed that LanD shares LanM's preference for

binding of larger REs (24). Unlike LanM, LanD lacks EF-hand sequence motifs, indicating a heretofore uncharacterized Ln^{III}-binding site.

The logic of periplasmic trafficking of lanthanide ions in lanthanide-utilizing bacteria is similarly uncharacterized. A Ln^{III}-metallophore complex has been inferred to be involved in uptake (24-28) and the likely solute-binding protein (META1p1778) for that complex has been isolated (24). LanM's preferential recognition of Nd^{III} and Sm^{III} has been studied extensively but its biological function is less well understood (17, 29). LanD (24) and another recently discovered protein, LanP (30), bind lanthanides but their functions are not established. How these players fit together is also unknown. Importantly, only La^{III}, Ce^{III}, Pr^{III}, and Nd^{III} (called "light lanthanides" herein) are imported efficiently into the cytosol in *M. extorquens* (24) to support lanthanide-dependent growth. In principle, this result could be explained by a metallophore or outer-membrane transporter (31) specific for these particular REs, but recent work implies such systems cannot alone account for the specificity of cytosolic lanthanide import (27, 32).

Herein, structural and biochemical studies of LanD reveal an unusual surface binding site with a metal coordination sphere that is only half-saturated by the protein. This allows LanD to form light lanthanide-selective dimers centered on a single metal ion. Two structure-guided substitutions invert dimerization selectivity and achieve separation factors of light lanthanides comparable to industrial extractants. Biochemical studies lead us to conclude that, physiologically, LanD's metal site is designed to disfavor self-dimerization while facilitating transfer of Ln^{III} ions to LanM. Therefore, characterization of LanD advances both biomolecular separations and understanding of lanthanide trafficking within cells.

RESULTS

LanD forms a metal-centered dimer

The X-ray crystal structure of LanD (UniprotKB C5B159) in the apo state (**Fig. 1A**, *SI Appendix* **Table S1**) reveals a compact three-helix bundle fold, stabilized by a disulfide linkage between helices 1 and 3 (α 1, α 3). The asymmetric unit contains two copies of LanD with a dimer interface, involving α 1 in each monomer, burying ~270 Å² of surface area (**Fig. 1A**). The apo dimer appears to be stabilized primarily via polar contacts, the most significant of which is a pair of symmetric inter-monomer salt-bridge interactions, involving Asp39 in one monomer and Arg47

in the other. Indeed, the behavior of the apoprotein in size-exclusion chromatography experiments (24) (SI Appendix, Figs. S2-S4) suggests a dimer at high protein concentration. In solution, the dimer is disrupted by high ionic strength, supporting the relevance of the crystallographically observed Asp39-Arg47 salt bridges (SI Appendix, Fig. S5).

To identify the putative Ln^{III}-binding motif in LanD, we co-crystallized the protein with La^{III}, the lightest Ln^{III} ion. This structure also revealed a dimer, but with an interface distinct from that of the apoprotein (**Fig. 1B**). We observed strong anomalous difference electron density map peaks for metal ions near a cluster of carboxylate side chains at the C-terminal end of the central α-helix (α2), proximal to the disulfide linkage (*SI Appendix*, **Fig. S6**). Unexpectedly, initial structures solved with 1:1 ratios of La^{III}:LanD revealed both a primary metal binding site and several auxiliary adventitious binding sites (*SI Appendix*, **Fig. S6**). Because the location of these metal-binding sites appeared to bridge a dimeric quaternary form, we decreased the metal:protein ratio to 0.5 in subsequent crystallization trials. These efforts yielded structures containing only a single metal ion bound at full occupancy at the interface between two LanD monomers (**Fig. 1B**).

Inspection of the metal binding site in La^{III}-LanD (0.5 equiv) shows a symmetric arrangement of three glutamate ligands contributed by each monomer, providing eight coordination interactions (Fig. 1C). In each monomer, the central bidentate Glu70 is flanked by two monodentate glutamates, Glu73 and Glu75. The ligands project out toward the exterior of the protein from the C-terminal end of $\alpha 2$ and the transition to $\alpha 3$. The metal-binding Glu residues and several other carboxylates in the second sphere undergo conformational change to form the metal-binding site when compared to their counterparts in the apo structure (SI Appendix, Figs. S7-S8). In La^{III}-LanD, a single water molecule, modeled at 0.5 occupancy, fills a ninth coordination site. Interestingly, LanD crystals contain only one monomer in the asymmetric unit, with the second half of the metal-linked dimer provided by a symmetry-related molecule in the crystal lattice, a phenomenon that underscores the C₂-symmetric arrangement of ligands. Analysis of the metal-centered dimer interface reveals that the coordination interactions nearly exclusively compose the dimer interface. The interface is not further stabilized by any significant hydrophobic contacts or hydrogen bonds involving other side chains. The lone exception is Arg69, which projects into the interface to stack against the monodentate ligand, Glu73, provided by the other monomer (Fig. 1D). This interaction may provide charge compensation for the unusual arrangement of the symmetric Glu73 ligands, in which a monodentate binding mode forces the non-coordinating side chain O atoms into very close proximity, only 2.5 Å apart. The Arg69 interaction is also symmetric, resulting in sandwiching of the Glu73 pair between the two second-sphere Arg side chains. The second sphere of the LanD metal binding site also exhibits an unusual number of flanking carboxylate side chains. Three additional Glu/Asp side chains (Asp77, Glu78, Glu81) cluster within ~10 Å of the metal binding site, all contributed by α3. The residue most proximal to the La^{III} ion, Glu78, appears to adopt multiple conformations (*SI Appendix*, **Fig. S9**). In one, the side chain projects close to the metal binding site, nearly overlapping with the coordinated water ligand. In the other conformer, the side chain is instead oriented away from the metal binding site. The multiple conformations of Glu78 and the presence of non-coordinated oxygen atoms with unsatisfied hydrogen bonding potential in ligands Glu73 and Glu75 could be consistent with a role in recognition of an exogenous ligand, such as another protein. Notably, the three metal ligands, Arg69, and Glu78 are among the few completely conserved residues in 263 LanD sequences predicted by BLAST (*SI Appendix*, **Figs. S10-S11**), underscoring the significance of the metal binding site and its unusual second sphere.

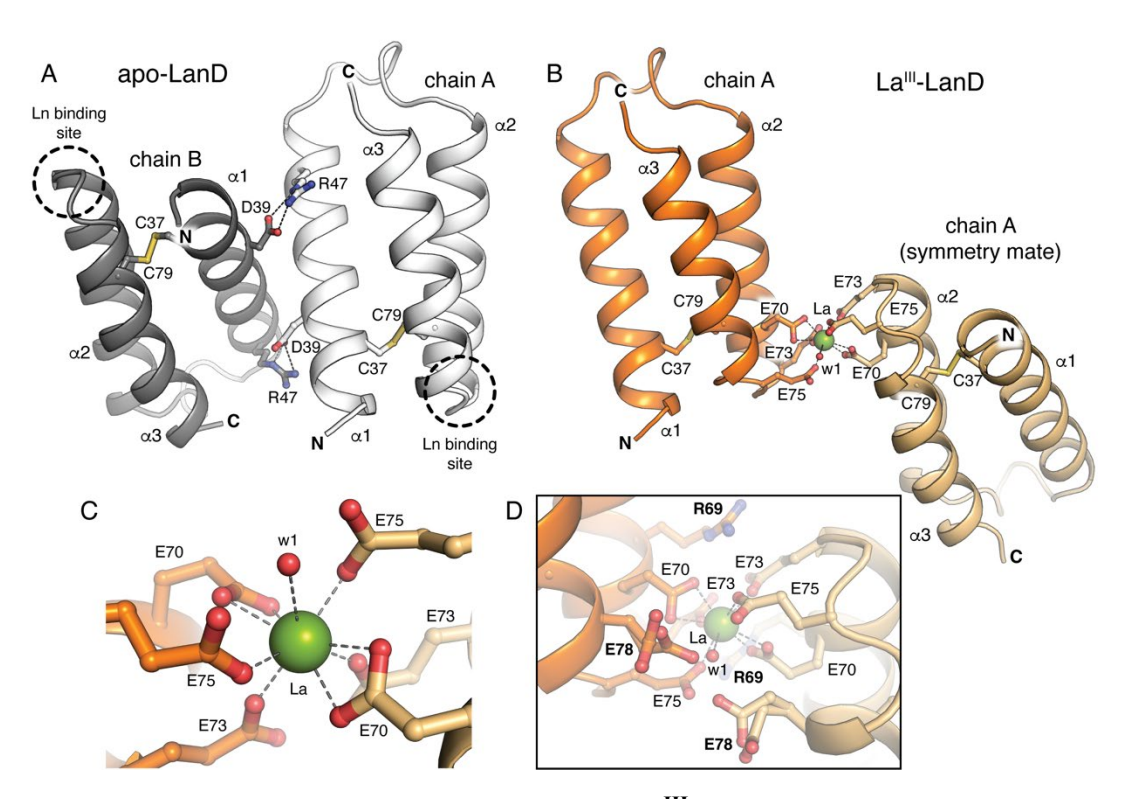


Figure 1. X-ray crystal structures of apo- and La^{III}-bound LanD reveal a metal-centered dimer. (A) X-ray crystal structure of the apo-LanD dimer showing the disulfide-stabilized three-helix bundle fold and the apo dimer interface, stabilized by hydrogen bonds between Asp39 in one monomer and Arg47 in the other. The apo dimer interface is located on the first helix, away from

the Ln^{III} binding site. "N" and "C" denote the N- and C-termini, respectively. (B) Overall view of the La^{III}-LanD structure showing the lanthanide-binding site near the end of helix 2. (C) Enlarged depiction of the La^{III} site in LanD. Dashed lines show coordination bonds. (D) View of key second-sphere amino acids near the lanthanide-binding site in La^{III}-LanD. The metal binding site is surrounded by additional polar side chains, including the strictly conserved residues, Arg69 and Glu78.

Dimer affinity and structure are lanthanide sensitive

The crystallographic observation of both metal-independent and metal-centered dimerization motivated determination of the equilibrium constants for dimer dissociation ($K_{\rm dimer}$) for LanD. We used isothermal titration calorimetry, an approach previously applied to measure metal-dependent dimerization in *Hans*-LanM (19). Characterization of apo-LanD dimer dissociation shows an endothermic response, fitting to $K_{\rm dimer} = 0.61$ mM (SI Appendix, **Fig. S12**, **Table S2**). $K_{\rm dimer}$ values for D39S and R47K variants were measured to be 0.80 and 1.06 mM, respectively (SI Appendix, **Figs. S13-S14**, **Table S2**), supporting the relevance of these residues' interaction in the dimer in solution. In the case of the holoprotein, the $K_{\rm dimer}$ values increased as ionic radius decreased, from 120 μ M for La^{III} to ~1 mM for Eu^{III} and Ho^{III} (**Fig. 2A**; SI Appendix, **Table S3**, **Figs. S15-S19**). The $K_{\rm dimer}$ values in the presence of Eu^{III} and Ho^{III} are endothermic and more similar to that of the apoprotein, suggesting that these ITC-determined $K_{\rm dimer}$ values may reflect both metal-dependent and metal-independent dimerization; nevertheless, the magnitude of the Eu^{III} $K_{\rm dimer}$ value is supported by luminescence studies (*vide infra*).

To investigate LanD's preference for the largest lanthanides in forming metal-centered dimers, we solved X-ray structures of the protein with Ce^{III} , Eu^{III} , and Ho^{III} , all at ratios of 0.5 metal:protein. All exhibit the same symmetry-related metal-centered dimer observed in the La^{III}-LanD structure. Ce^{III} neighbors La^{III} on the periodic table and is most similar in size. The Ce^{III} binding site resembles the La^{III} binding site, including the exogenous solvent ligand (**Fig. 2B**). The most significant difference is a diminished occupancy for this water (0.35 in Ce^{III} -LanD versus 0.49 in La^{III}-LanD) (*SI Appendix*, **Fig. S20**). This difference in water occupancy may reflect the smaller ionic radius of Ce^{III} that may not as readily accommodate a ninth ligand. Consistent with this prediction, structures of LanD with smaller lanthanides, Eu^{III} and Ho^{III} , show complete loss of the solvent ligand (**Figs. 2C, 2D**). The increase in K_{dimer} with decreasing ionic radius appears to correlate with loss of the coordinated solvent molecule observed at partial occupancy in the structures of La^{III}- and Ce^{III} -LanD. We hypothesize that, as the ionic radius of the lanthanide ions

contracts from La^{III} to Ho^{III}, increasing steric and charge repulsion between the multiple carboxylates at the dimer interface yields a smaller coordination number and favors dimer dissociation.

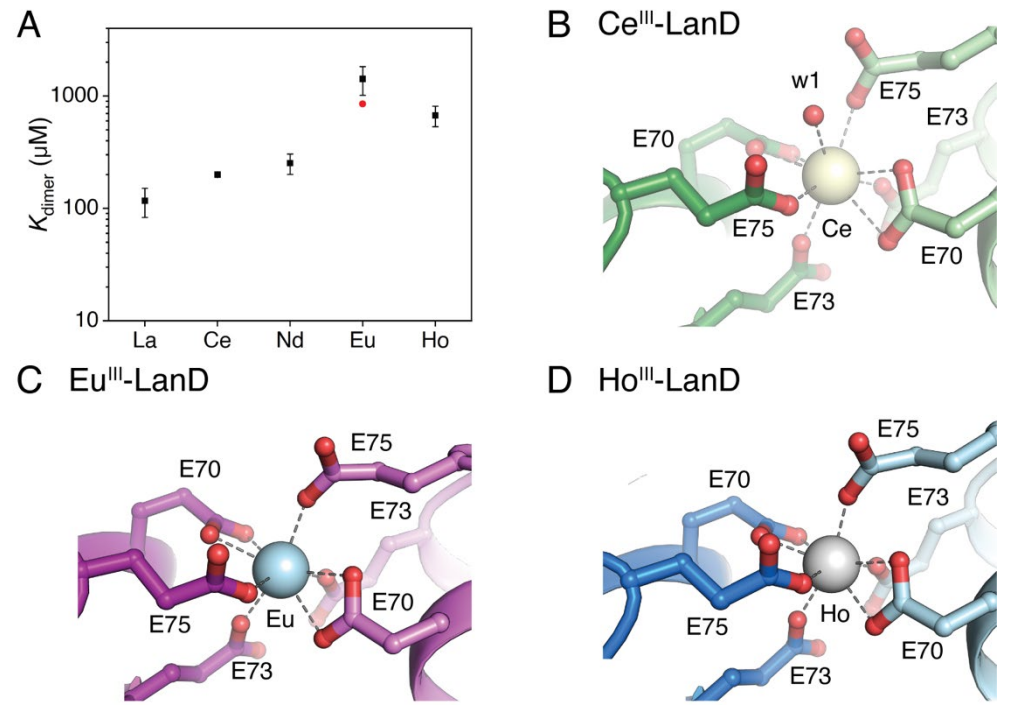


Figure 2. Biochemical and structural analysis of lanthanide-sensitive dimerization. (A) Dimer dissociation constants (K_{dimer} values, black squares) for La^{III}-, Ce^{III}-, Nd^{III}-, Eu^{III}-, and Ho^{III}-LanD, determined by ITC. The K_{dimer} for metal-dependent dimerization of Eu^{III}-LanD as determined by luminescence lifetime analysis is shown as a red circle. (B-D) Comparison of the metal-binding sites across a series of lanthanides bound to LanD. Contraction of the ionic radius across the lanthanide series results in loss of coordinated solvent and shorter metal-ligand bonds.

LanD monomer favors $Nd^{\rm III}$, $Sm^{\rm III}$, and $Eu^{\rm III}$ binding

Despite the intriguing self-dimerization phenomenon, the K_{dimer} values reported above likely are not tight enough to be relevant in the cell, which would leave LanD monomeric and the Ln^{III} ion coordination spheres only partially satisfied by protein ligands. To support this interpretation, we examined the dependence of Eu^{III} luminescence lifetime on protein concentration. The number of water molecules (q) in the first coordination sphere of Eu^{III} can be estimated based on its luminescence lifetime (33-35). Fully aquated Eu^{III} has 8-9 ligands (average of 8.3) (36). At 20 μ M LanD, where the monomer dominates and Eu^{III} is fully protein bound (*SI Appendix*, **Fig. S21**), q = 4.1, while at 350 μ M, q decreases to 2.6 (**Fig. 3A**). Assuming that the

holodimer has no coordinated solvent (q = 0) based on the X-ray structure of Eu^{III}-LanD, at 350 μ M LanD, ~65% of the protein units are monomeric in solution, yielding $K_{\text{dimer}} = 850 \,\mu$ M for Eu^{III}-dependent dimerization. These results validate the interpretation of the ITC-derived K_{dimer} values, and they confirm that solvent provides approximately half of the coordination sphere for Eu^{III} bound to the LanD monomer.

Therefore, we sought to determine the metal affinities (K_{d1}) of the more physiologically relevant monomer. The weak K_{dimer} value for Eu^{III} allowed use of ITC to determine K_{d1} for Eu^{III}-LanD to be 340 nM, with a stoichiometry of 1.0 (SI Appendix, **Fig. S22**, **Table S4**). The relative K_{d1} values for other Ln^{III} ions were estimated by direct competition with Eu^{III}, taking advantage of the higher luminescence intensity of protein-bound vs. unbound Eu^{III} ion, and converted into absolute K_{d1} values using the ITC-determined K_{d1} for Eu^{III} (**Fig. 3B**; SI Appendix **Fig. S23**, **Table S5**). These values are substantially tighter than the K_{dimer} values and show an opposite trend in sensitivity to RE identity, with affinity increasing from La^{III} to Nd^{III}, plateauing, and then decreasing beyond Eu^{III}. Thus, the LanD monomer favors binding of lanthanide ions that are less preferred for supporting methylotrophic growth.

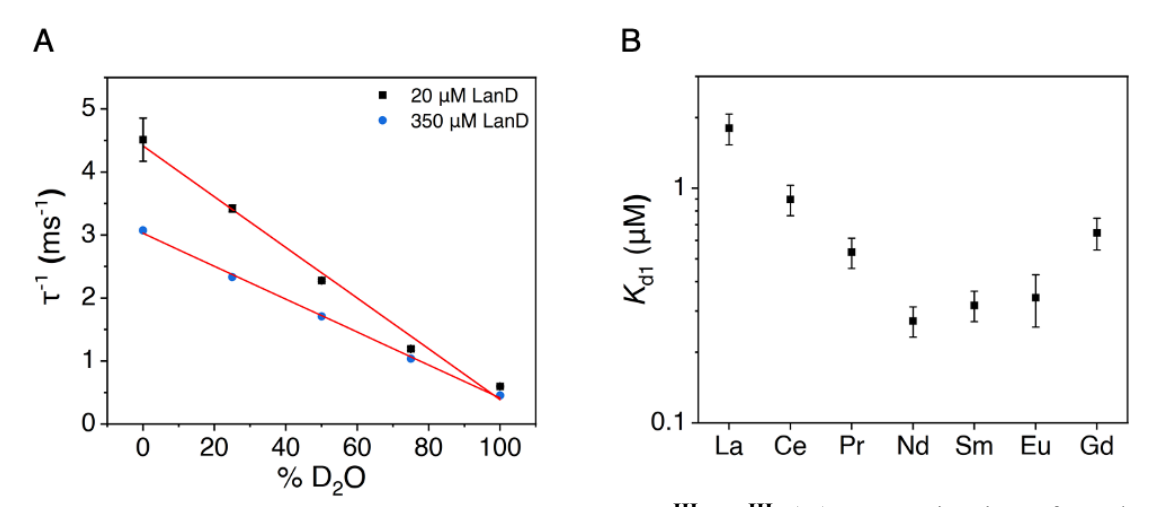


Figure 3. LanD monomer preferentially binds Nd^{III} -Eu^{III}. (A) Determination of q values for 20 and 350 μ M Eu^{III}-LanD, supporting coordination with ~4 solvent molecules in the monomeric state. (B) Plot of K_{d1} values for Ln^{III}-LanD.

Engineering LanD for dimer-mediated separations

We first sought to apply the above structural and biochemical insights to separations. Although wild-type LanD's metal-centered dimerization is weak, we envisioned that its interfacial metal site could be exploited by re-engineering LanD to dimerize selectively in the presence of

higher-value Pr^{III} and Nd^{III} over La^{III} and Ce^{III} . We reasoned that this goal would require weakening metal binding to monomer (K_{d1}) in general and tightening K_{dimer} selectively for Pr^{III} and Nd^{III} , which would likely involve overcoming steric constraints to preferentially stabilize an octacoordinate metal site (SI Appendix, **Fig. S24**). This approach would make K_{dimer} for preferred elements tighter than K_{d1} for non-preferred elements, an arrangement fundamentally distinct from the dimerizing Hans-LanM system, where K_{d1} is much tighter (picomolar) than K_{dimer} (high nanomolar to low micromolar) (19).

To weaken K_{d1} , we mutated one of the monodentate carboxylate ligands, Glu75, to Gln (E75Q) (SI Appendix, Fig. S24). Competition assays against xylenol orange show qualitatively that K_{d1} values in E75Q are weaker than in wild-type LanD (SI Appendix, Table S6, Fig. S25). ITC studies indicated a K_{d1} value for Eu^{III}-LanD-E75Q of 0.88 μ M with n=1, indicating a monomer under these conditions, and a titration of 50 μ M E75Q with Eu^{III} followed by luminescence yields 1:1 stoichiometry, suggesting that K_{dimer} is still substantially weaker than K_{d1} (SI Appendix, Fig. S26). Luminescence competition experiments were used to determine the trend in K_{d1} values for La^{III} to Gd^{III}, which is similar to that of wild-type LanD (Fig. 4A; SI Appendix, Fig. S27).

We next reasoned that removing the steric and charge repulsion near the metal site arising from the outer-sphere residue that occupies two conformations in the X-ray structures, Glu78, might strengthen dimerization, particularly for smaller lanthanide ions. We constructed an E78A variant in the E75Q background. Interestingly, competition assays with xylenol orange were consistent with stoichiometries of 0.5, suggesting substantial dimerization under the experimental conditions (10 μ M protein) and therefore that K_{dimer} is now in the low micromolar range (*SI Appendix*, **Fig. S28**). Indeed, time-resolved luminescence titration of 10 μ M LanD-E75Q/E78A with Eu^{III} showed an endpoint at 0.5 equivalents. Competitive titrations of this presumptive Eu^{III} bridged dimer showed that La^{III} and Ce^{III} competed poorly – with 50-60 μ M of these metal ions required to outcompete Eu^{III} binding by 50% (resulting in a decrease of Eu^{III} luminescence) – whereas ~20 μ M Pr^{III} and ~10 μ M Nd^{III} were required (**Fig. 4B**). The K_{dimer} values were measured by ITC for the complexes with La^{III}–Nd^{III} (*SI Appendix*, **Figs. S29-S32**), validating this result (**Fig. 4A**, *SI Appendix* **Table S7**). K_{d1} s could not be measured by ITC because K_{dimer} s are on the order of typical protein concentrations, but we propose that they may be similar to those with E75Q. Therefore, we believe we have achieved K_{dimer} in the range of K_{d1} . Remarkably, from these two

substitutions, the affinities of the Ln^{III}-induced dimers are increased by 10- to 100-fold compared to the wild-type LanD. This pattern shows that large selectivity effects can be achieved from even simple substitutions at the LanD interface.

These results encouraged us to investigate the ability of LanD-E75Q/E78A to separate light lanthanides, La^{III}-Nd^{III}, from one another. We used spin concentrators with a 10-kDa cutoff membrane for small-scale separation tests with pairs of Ln^{III} ions, envisioning that Nd^{III} and Pr^{III} would preferentially induce dimerization (~14 kDa) and would be less likely to flow through the filter. The separation factors (SFs) were determined from the ratios of the distribution coefficients of each metal between retentate and flowthrough (see *SI* Methods). We tested pH 5 and 6 and varied starting protein concentration and metal:protein stoichiometry (*SI Appendix*, Figs. S33-S34) and found that 3:1 monomer:target metal (Pr^{III} or Nd^{III}) yielded the best SFs. Wild-type LanD has poor SFs (*SI Appendix*, Fig. S35). LanD-E75Q/E78A, however, achieved up to 70-80% recovery of Pr^{III} and Nd^{III} in the retentate and 60-80% partitioning of La^{III} to flowthrough (Fig. 4C). When equal concentrations of La^{III}, Ce^{III}, Pr^{III}, and Nd^{III} were used together, the SFs were similar to those obtained in binary element experiments (Table 1; *SI Appendix*, Table S8). These SFs are higher than for common industrial extractants DEHPA and PC88A (37). Advantageously, the entire LanD process of incubation and filtration takes <1 h, as opposed to many synthetic ligands for which SFs are reported at 24 h (6, 38).

Table 1. Separation factors for LanD-E75Q/E78A (5 μ M), filtration, separation of mixture of 0.8 μ M each La^{III}, Ce^{III}, Pr^{III}, Nd^{III}.

	La ^{III}	Ce ^{III}	Pr ^{III}	Nd ^{III}
La ^{III}	1	3.0 ± 0.4	5.1 ± 0.6	7.3 ± 0.9
Ce^{III}		1	1.7 ± 0.2	2.4 ± 0.3
Pr^{III}			1	1.4 ± 0.2
Nd^{III}				1

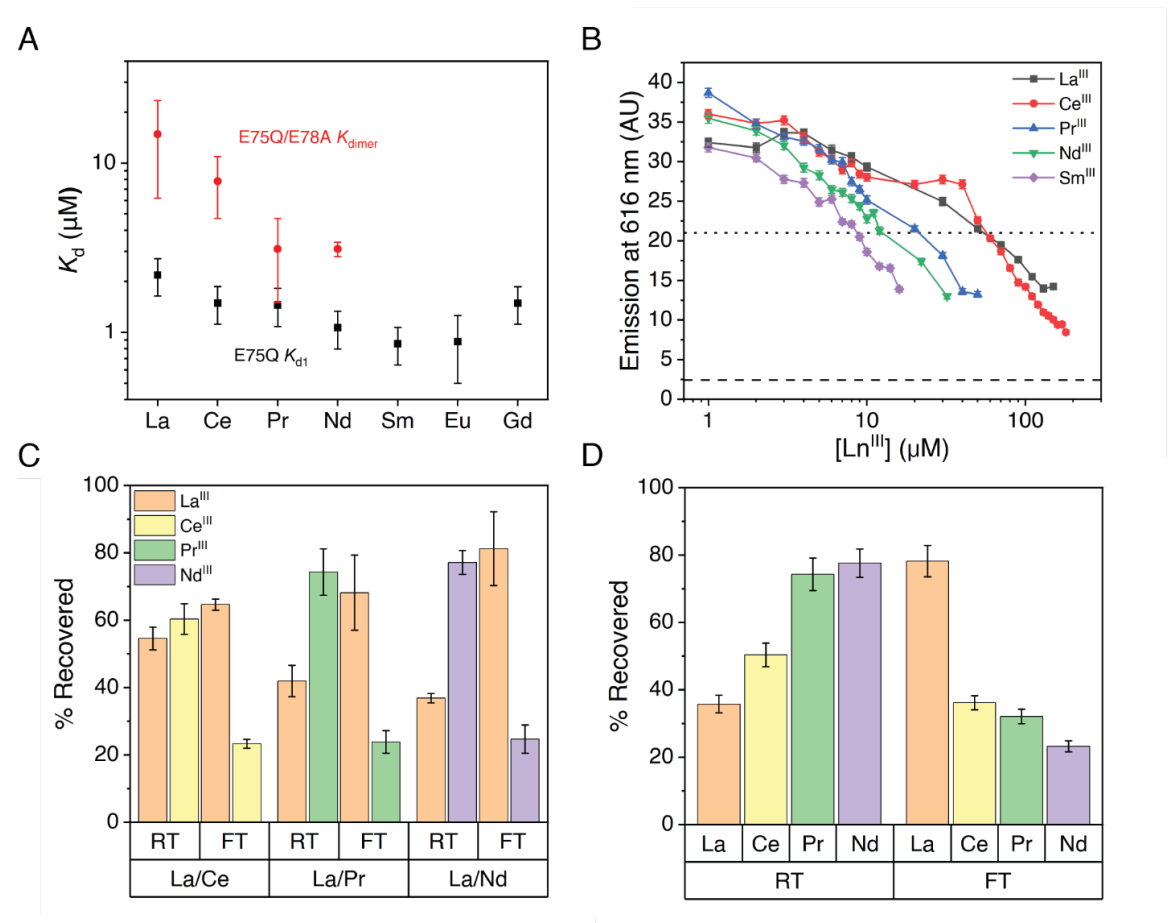


Figure 4. Interfacial mutations enable light lanthanide separations. (A) K_{d1} for each Ln^{III} ion relative to Eu^{III} for LanD-E75Q, from competitive luminescence titrations (black squares), K_{dimer} values for LanD-E75Q/E78A, measured by ITC (red circles). (B) Luminescence competition titration with 10 μM LanD-E75Q/E78A loaded with 0.5 equiv. Eu^{III} and titrated with other Ln^{III} ions. Samples prepared in 20 mM Tris, 100 mM KCl, pH 7.0 buffer. (C) Binary separations of light lanthanides using LanD-E75Q/E78A; RT = retentate, FT = flowthrough. The SFs are: $SF_{Ce/La} = 3.1 \pm 0.4$. $SF_{Pr/La} = 5.1 \pm 1.3$. $SF_{Nd/La} = 6.9 \pm 1.5$. Protein (5 μM), 1.7 μM each Ln^{III} ion, in 20 mM MES, 100 mM KCl, pH 6.0. (D) Separations with an equimolar mixture of $La^{III} - Nd^{III}$. See **Table 1** for SFs.

LanD interacts with apo-LanM

The observation of a higher-affinity dimer in LanD-E75Q/E78A reinforces the notion that the conserved, highly negatively charged environment of the metal site serves to disfavor dimerization in the wild-type protein. Therefore, we sought to obtain insight into LanD's biological function in light of this unusual surface metal site. We first considered the possibility that the coordination sphere of a LanD-bound Ln^{III} ion might be completed in a ternary complex with another multidentate ligand. We investigated several chelators of potential in vivo periplasmic

relevance and found no evidence of ternary complex formation (*SI Appendix* Discussion, **Fig. S36-S38**). Therefore, we considered that the surface site might enable rapid transfer of Ln^{III} ions between LanD and other periplasmic proteins encoded by the lanthanide uptake gene cluster. The similarity in affinity trends of LanD's K_{d1} values and $K_{d,app}$ values of LanM (**Fig. 3B**; *SI Appendix*, **Fig. S39**) motivated investigation of a potential LanD-LanM interaction. Mixing of La^{III}-LanD and LanM (in the form of the Ln^{III}-responsive fluorescent sensor, LaMP1 (24)) shows rapid transfer of La^{III} to LanM (*SI Appendix*, **Fig. S40**). Because LanD's K_{d1} values are 10^5 - to 10^6 -fold weaker than those of LanM (17), however, this result does not necessarily indicate direct transfer. We examined interaction of apo-LanM with apo-LanD using ITC. We used apo-LanD rather than holo-LanD to avoid large heats associated with LanM metalation (17) and because the structures of apo- and holo-LanD are similar. Interestingly, the two proteins interact with $K_d = 4.0 \pm 1.9 \,\mu$ M and 1:1 stoichiometry ($n = 1.2 \pm 0.2$), parameters that suggest a physiologically relevant interaction (**Fig. 5**; *SI Appendix*, **Fig. S41**, **Table S9**).

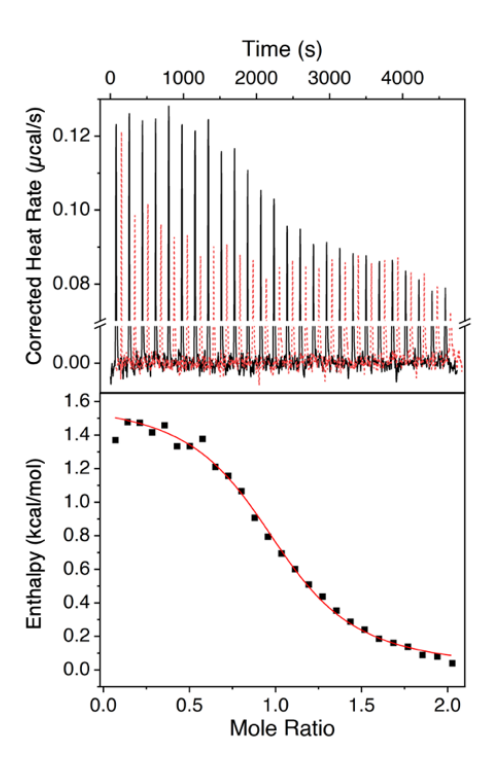


Figure 5. LanD interacts with apo-LanM. ITC titration of apo-LanD with apo-LanM. Top plot shows raw data for representative titrations of 240 μM apo-*Mex*-LanM into 30 μM apo-LanD (black) and into buffer (control, red dashes, offset by 75 s for clarity). Bottom plot shows binding isotherm after subtraction of the control titration; the x-axis denotes the molar ratio of LanM added to LanD. The fit is to an independent model with parameters presented in **Table S9**. Conditions: 30 mM MOPS, 100 mM KCl, pH 7.0, 25 °C.

If LanD were to transfer Ln^{III} ions to LanM inside the cell, one would expect LanD may not interact as tightly with Ln^{III}-bound LanM. Indeed, titration of apo-LanD with Sm^{III}₃-LanM (Sm^{III} being favored by both LanM and LanD) shows no evidence of interaction (*SI Appendix*, **Fig. S42**). Because apo-LanMs characterized to date are primarily intrinsically disordered and therefore might be able to complex non-specifically with other proteins, we titrated apo-*Mex*-LanD with apo-*Hans*-LanM, which also provided no evidence of interaction (*SI Appendix*, **Fig. S43**). The specific interaction of LanD with apo-*Mex*-LanM suggests that LanM is the exogenous ligand that the Ln^{III}-LanD site recognizes in vivo, with the function of that recognition being transfer of Ln^{III} ions from LanD to LanM. This model implies a chaperone function for LanD.

DISCUSSION

M. extorquens LanD is only the third class of biological lanthanide-binding site to be structurally characterized, after the Ln-dependent alcohol dehydrogenases (39, 40) and lanmodulins (19). Unlike these previously crystallographically characterized sites, LanD is structurally unrelated to known biological ligands for Ca^{II}. Three residues, one bidentate carboxylate flanked by two monodentate carboxylates, provide just four of the requisite eight to nine ligands for the bound lanthanide ion. The LanD metal-binding site does not allow for coordination from backbone atoms (unlike in LanMs; SI Appendix, Fig. S44) and, as a result of the coordination environment not being saturated by ligands from a monomeric unit, a face-to-face arrangement of carboxylates from two protomers is observed in the crystal structure of the metalbridged dimer. The excessive negative charge of the dimeric metal site is enhanced by several additional nearby negatively charged residues, including the second-sphere, conserved residue Glu78, implicated in destabilizing the metal-dependent dimer interface. The importance of charge at this interface is reinforced by the strong enhancement of K_{dimer} induced by the inner-sphere E75Q and outer-sphere E78A substitutions. Because Ln^{III} ions favor high coordination numbers, a surface site only half-coordinated by protein residues would be prone to self-dimerization with another protein monomer, but we propose that the charge repulsion of wild-type LanD metal site serves to disfavor this process.

LanD's C₂-symmetric dimer centered on a single metal ion is a relatively simple scaffold from which to design metal sites that can discern between elements by exploiting differences in

ionic radius, hydration, and coordination number, as our separations work demonstrates. As a single ligand, LanD's aqueous SFs are higher than common extractants DEHPA and PC88A (37) and comparable to next-generation diglycolamide extractants, typically implemented in liquidliquid extraction schemes (3, 14, 41), where the lanthanide ion partitions between an organic phase with an organic extractant and an aqueous phase (SI Appendix Table S10) (42). They are also similar to other dimerizing ligand systems, such as a supramolecular encapsulation approach $(SF_{Nd/La} = 6)$ (38) that is conceptually similar to LanD's metal-centered dimerization, and the dimerizing TriNOx ligands (SF_{La/Nd} \sim 10) (15, 43). LanD's SFs are lower than the "tug-of-war" systems using two or more chelators, particularly macrophosphi, which has the highest SF for adjacent lanthanides, although they are more similar after accounting for the contribution of the other chelators present (DEHPA and lactic acid) (9). However, the recent LanM-based column systems, which are also single-ligand and all-aqueous, may be more appropriate points of direct comparison than two-phase, multi-ligand systems. LanD's SFs substantially outperform both the original Mex-LanM column and the improved Hans-LanM column in the La-Nd range (SI Appendix Table S10) (19, 44), and LanD's weaker metal binding under milder conditions could also be favorable for rapid separations. The small number of inter-monomer interactions beyond LanD's metal-binding site suggests that this interface could be engineered to further amplify dimer affinity and RE/RE selectivity, as well as shift selectivity trends to access separations of smaller REs. Tethering of the dimers together (covalently or non-covalently) and immobilization on a column or porous membrane (45) could yield sterically congested metal sites that would strongly disfavor binding of La^{III} and Ce^{III}. Furthermore, the rigid, disulfide bridged structure of LanD may be a good candidate for simplification to a cyclic peptide (46).

The unusual properties of LanD, in particular surface accessibility and affinity trends of its metal site, also provided insights into lanthanide trafficking in the cell, leading us to experiments strongly suggesting that a physiological function of LanD is to transfer Ln^{III} ions to LanM. The interaction and directional transfer of Ln^{III} ions between these proteins restricts the possible mechanisms of lanthanide trafficking in the periplasm given the other activities encoded in the cluster (31). In particular, the observation that both proteins prefer not the biologically preferred La^{III} and Ce^{III} but rather Nd^{III} and Sm^{III} (17, 19) – which are less favored in biology but still abundant in the environment and therefore need to be withheld from lanthanide-dependent enzymes (32, 47, 48) – is crucial. Outer-membrane uptake of Ln^{III} ions via a presumptive Ln^{III}-

metallophore complex is promiscuous (24-27, 49, 50), necessitating an additional source of selectivity to account for the sharp and nearly complete cutoff in cytosolic uptake between Nd^{III} and Sm^{III} (24).

A pathway with selectivity opposite that of lanthanide preference of enzyme metalation would fit the bill for being able to "siphon" off the less-desirable lanthanides, which incidentally would mean that Ln^{III} ions must be released from the metallophore in the periplasm so that sorting can take place. We propose that the LanD-LanM axis is (part of) this siphon, leaving the larger REs to be imported to the cytosol and the smaller REs transferred from LanD to LanM for sequestration in the periplasm or, possibly, export (29). This model would explain why the *Beijerinckiaceae* equivalents of *lanD* and *lanM* are upregulated to a greater extent in the presence of Nd^{III} than of La^{III} (51). The functional connectivity between LanD and LanM is also supported by the observation that in the 263 organisms in which LanD orthologs were identified by BLAST search (*SI Appendix*, **Fig. S10**), we were able to identify LanM orthologs in all but 6 (and 3 of those had LanMs annotated in organisms in the same genus). We suggest that the other ~450 LanMs identified to date may have LanD equivalents that are structurally distinct from *M. extorquens* LanD but fulfill a similar function (perhaps with different metal selectivities). Although LanD and LanM are not required for growth on La^{III} (26), our proposal predicts that both might be particularly important in the presence of non-preferred REs such as Sm^{III}.

In summary, LanD's unusual coordination environment exemplifies how to achieve high selectivity between lanthanides even with binding affinities much weaker than those of LanMs and many small-molecule chelators, and it inspires new models for cellular lanthanide trafficking. Finally, our engineering work shows the potential of metal-centered dimerization to achieve biomolecular chelators with high separation ability within the lanthanide series and potentially other parts of the periodic table.

Materials and Methods. The expression, purification, and in vitro characterization of wild-type LanD and its E75Q and E75Q/E78A variants are described in the SI Appendix. This information includes methods and data for crystallographic structure determination of apo-, La^{III}-, Ce^{III}-, Eu^{III}, and Ho^{III}-LanD. The SI Appendix also contains detailed methods, chromatograms, spectra, and full thermodynamic parameters derived from ITC- and luminescence-based metal and protein titration experiments for K_{dimer} and K_{dl} determinations for LanD and its variants, as well as for studies of the LanD-LanM interaction. Methods and supporting data for LanD-based separation experiments are also described. Finally, the SI Appendix also includes methods and data for

luminescence-based titrations to assess potential ternary complex formation in LanD with small molecules, the results of which are also treated in a Supplementary Discussion section in the SI Appendix.

Data, Materials, and Software Availability. All data required for evaluation of the conclusions of this manuscript, and all experimental protocols, are provided in the main text and/or SI Appendix. Materials (i.e., plasmids) for expression of the proteins discussed herein are available from J.A.C. upon request pending scientific review and a completed material transfer agreement. The atomic coordinates for LanD x-ray crystal structures have been deposited in the Protein Data Bank, www.pdb.org (PDB ID: 9C8W, 9C8X, 9C8Y, 9C8Z, 9C90).

Acknowledgments. Functional characterization work was financially supported by the U.S. National Science Foundation under award CHE-1945015 (to J.A.C.) and engineering and separation work was funded by the DARPA Environmental Microbes as a Bioengineering Resource (EMBER) program (contract DE-AC52-07NA27344). W.B.L. acknowledges a National Defense Science and Engineering Graduate fellowship. A.K.B. acknowledges National Institutes of Health grant GM119707 and C.-Y.L. acknowledges a fellowship from the Jane Coffin Childs Memorial Fund for Medical Research. This research used resources of the Advanced Photon Source, a DOE Office of Science User Facility operated by Argonne National Laboratory under contract number DE-AC02-06CH11357. Use of the Life Sciences Collaborative Access Team Sector 21 was supported by the Michigan Economic Development Corporation and the Michigan Technology Tri-Corridor (grant 085P1000817). This research also used resources at beamline 17 of the National Synchrotron Light Source II, a U.S. Department of Energy (DOE) Office of Science User Facility operated for the DOE Office of Science by Brookhaven National Laboratory under Contract No. DE-SC0012704. The Center for BioMolecular Structure (CBMS) at NSLS-II is primarily supported by the National Institutes of Health, National Institute of General Medical Sciences (NIGMS) through a Center Core P30 Grant (P30GM133893), and by the DOE Office of Biological and Environmental Research (KP1607011). Use of the Stanford Synchrotron Radiation Lightsource, SLAC National Accelerator Laboratory, is supported by the U.S. Department of Energy, Office of Science, Office of Basic Energy Sciences under Contract No. DE-AC02-76SF00515. The SSRL Structural Molecular Biology Program is supported by the DOE Office of Biological and Environmental Research, and by the National Institutes of Health, National Institute of General Medical Sciences (P30GM133894). We acknowledge National Institutes of Health SIG awards S10-OD0215145 for isothermal titration calorimetry instrumentation and S10-OD030490 for the SEC-MALS-dynamic light scattering system. The views, opinions, and/or findings expressed are those of the authors and should not be interpreted as representing the official views or policies of the Department of Defense or the U.S. Government. Approved for public release, distribution unlimited. We are grateful to J. Seidel and D.M. Park (LLNL) and E. Boros (Wisconsin) for discussions, and we thank D. Carkner (Penn State) for experimental assistance.

Author Contributions. All authors designed research; W.B.L., J.J.J., and C.-Y.L. performed research; W.B.L. contributed new reagents/analytic tools; and W.B.L., J.J.J., A.K.B., and J.A.C. wrote the paper. All authors reviewed the results and edited the manuscript, and all authors approved the final version of the manuscript.

Competing interests statement. The authors declare the following competing financial interest(s): W.B.L., J.J.J., C.-Y.L., A.K.B., and J.A.C. are inventors on patent applications filed by the Pennsylvania State University related to this work. J.A.C. is a co-founder and holds equity in REEterra, Inc.

REFERENCES

- 1. D. S. Sholl, R. P. Lively, Seven chemical separations to change the world. *Nature* **532**, 435-437 (2016).
- 2. K. L. Nash, M. P. Jensen, Analytical-scale separations of the lanthanides: A review of techniques and fundamentals. *Sep. Sci. Technol.* **36**, 1257-1282 (2001).
- 3. F. Xie, T. A. Zhang, D. Dreisinger, F. Doyle, A critical review on solvent extraction of rare earths from aqueous solutions. *Miner. Eng.* **56**, 10-28 (2014).
- 4. Z. C. Sims *et al.*, How Cerium and Lanthanum as Coproducts Promote Stable Rare Earth Production and New Alloys. *J. Sustain. Met.* **8**, 1225-1234 (2022).
- 5. U. S. Geological Survey (2024) Mineral Commodity Summaries 2024. (Reston, VA).
- 6. M. R. Healy *et al.*, Efficient separation of light lanthanides(III) by using bis-lactam phenanthroline ligands. *Chem. Eur. J.* **25**, 6326-6331 (2019).
- 7. R. M. Pallares, S. Hébert, M. Sturzbecher-Hoehne, R. J. Abergel, Chelator-assisted high performance liquid chromatographic separation of trivalent lanthanides and actinides. *New J. Chem.* **45**, 14364-14368 (2021).
- 8. K. R. Johnson, D. M. Driscoll, J. T. Damron, A. S. Ivanov, S. Jansone-Popova, Size Selective Ligand Tug of War Strategy to Separate Rare Earth Elements. *JACS Au* 3, 584-591 (2023).
- 9. N. A. Thiele, D. J. Fiszbein, J. J. Woods, J. J. Wilson, Tuning the separation of light lanthanides using a reverse-size selective aqueous complexant. *Inorg. Chem.* **59**, 16522-16530 (2020).
- 10. A. Roca-Sabio *et al.*, Macrocyclic Receptor Exhibiting Unprecedented Selectivity for Light Lanthanides. *J. Am. Chem. Soc.* **131**, 3331-3341 (2009).
- 11. A. Hu, S. N. MacMillan, J. J. Wilson, Macrocyclic Ligands with an Unprecedented Size-Selectivity Pattern for the Lanthanide Ions. *J. Am. Chem. Soc.* **142**, 13500-13506 (2020).
- 12. H. Fang *et al.*, Electro-kinetic separation of rare earth elements using a redox-active ligand. *Angew. Chem. Int. Ed.* **56**, 13450-13454 (2017).
- 13. K. P. Ruoff *et al.*, Mediating Photochemical Reaction Rates at Lewis Acidic Rare Earths by Selective Energy Loss to 4f-Electron States. *J. Am. Chem. Soc.* **145**, 16374-16382 (2023).
- 14. G. A. Picayo, M. P. Jensen, "Rare earth separations: Kinetics and mechanistic theories" in Handbook on the Physics and Chemistry of Rare Earths: Including Actinides, J.-C. G. Bünzli, V. K. Pecharsky, Eds. (North-Holland, Oxford, 2018), vol. 54.
- 15. J. A. Bogart *et al.*, Accomplishing simple, solubility-based separations of rare earth elements with complexes bearing size-sensitive molecular apertures. *Proc. Natl. Acad. Sci. U.S.A.* **113**, 14887-14892 (2016).
- 16. R. F. Higgins, K. P. Ruoff, A. Kumar, E. J. Schelter, Coordination Chemistry-Driven Approaches to Rare Earth Element Separations. *Acc. Chem. Res.* **55**, 2616-2627 (2022).

- 17. J. A. Cotruvo, Jr., E. R. Featherston, J. A. Mattocks, J. V. Ho, T. N. Laremore, Lanmodulin: A highly selective lanthanide-binding protein from a lanthanide-utilizing bacterium. *J. Am. Chem. Soc.* **140**, 15056-15061 (2018).
- 18. Z. Dong *et al.*, Bridging hydrometallurgy and biochemistry: A protein-based process for recovery and separation of rare earth elements. *ACS Cent. Sci.* 7, 1798-1808 (2021).
- 19. J. A. Mattocks *et al.*, Enhanced rare-earth separation with a metal-sensitive lanmodulin dimer. *Nature* **618**, 87-93 (2023).
- 20. T. S. Choi, F. A. Tezcan, Overcoming universal restrictions on metal selectivity by protein design. *Nature* **603**, 522-527 (2022).
- 21. B. Maniaci *et al.*, Design of High-Affinity Metal-Controlled Protein Dimers. *Biochemistry* **58**, 2199-2207 (2019).
- 22. G. J.-P. Deblonde *et al.*, Selective and efficient biomacromolecular extraction of rare-earth elements using lanmodulin. *Inorg. Chem.* **59**, 11855-11867 (2020).
- 23. J. A. Seidel, P. Diep, Z. Dong, J. A. Cotruvo, Jr., D. M. Park, EF-hand battle royale: hetero-ion complexation in lanmodulin. *JACS Au*, in revision.
- 24. J. A. Mattocks, J. V. Ho, J. A. Cotruvo, Jr., A selective, protein-based fluorescent sensor with picomolar affinity for rare earth elements. *J. Am. Chem. Soc.* **141**, 2857-2861 (2019).
- 25. A. M. Ochsner *et al.*, Use of rare earth elements in the phyllosphere colonizer *Methylobacterium extorquens* PA1. *Mol. Microbiol.* **111**, 1152-1166 (2019).
- 26. P. Roszczenko-Jasińska *et al.*, Gene products and processes contributing to lanthanide homeostasis and methanol metabolism in *Methylorubrum extorquens* AM1. *Sci. Rep.* **10**, 12663 (2020).
- 27. A. M. Zytnick *et al.*, Identification and characterization of a small-molecule metallophore involved in lanthanide metabolism. *Proc. Nat. Acad. Sci. U.S.A.* **121**, e2322096121 (2024).
- 28. C.-E. Wegner, L. Gorniak, S. Riedel, M. Westermann, K. Küsel, Lanthanide-Dependent Methylotrophs of the Family *Beijerinckiaceae*: Physiological and Genomic Insights. *Appl. Environ. Microbiol.* **86**, e01830-01819 (2019).
- 29. Y. Fujitani, T. Shibata, A. Tani, A Periplasmic Lanthanide Mediator, Lanmodulin, in *Methylobacterium aquaticum* Strain 22A. *Front. Microbiol.* **13** (2022).
- 30. J. L. Hemmann *et al.*, Lanpepsy is a novel lanthanide-binding protein involved in the lanthanide response of the obligate methylotroph *Methylobacillus flagellatus*. *J. Biol. Chem.* **299**, 102940 (2023).
- 31. E. R. Featherston, J. A. Cotruvo, Jr., The biochemistry of lanthanide acquisition, trafficking, and utilization. *Biochim. Biophys. Acta Mol. Cell Res.* **1868**, 118864 (2021).
- 32. L. Gorniak *et al.*, Changes in growth, lanthanide binding, and gene expression in *Pseudomonas alloputida* KT2440 in response to light and heavy lanthanides. *bioRxiv* 10.1101/2024.04.15.589537 (2024).
- 33. T. Kimura, G. R. Choppin, Y. Kato, Z. Yoshida, *Radiochim. Acta* 72, 61-64 (1996).
- 34. J. Bruno, W. D. Horrocks, R. J. Zauhar, Europium(III) luminescence and tyrosine to terbium(III) energy-transfer studies of invertebrate (octopus) calmodulin. *Biochemistry* **31**, 7016-7026 (1992).
- 35. D. Chaudhuri, W. D. Horrocks, J. C. Amburgey, D. J. Weber, Characterization of lanthanide ion binding to the EF-hand protein S100β by luminescence spectroscopy. *Biochemistry* **36**, 9674-9680 (1997).

- 36. A. Habenschuss, F. H. Spedding, The coordination (hydration) of rare earth ions in aqueous chloride solutions from x-ray diffraction. III. SmCl₃, EuCl₃, and series behavior. *J. Chem. Phys.* **73**, 442-450 (1980).
- 37. T. Sato, Liquid-liquid extraction of rare-earth elements from aqueous acid solutions by acid organophosphorus compounds. *Hydrometallurgy* **22**, 121-140 (1989).
- 38. J. G. O'Connell-Danes, B. T. Ngwenya, C. A. Morrison, J. B. Love, Selective separation of light rare-earth elements by supramolecular encapsulation and precipitation. *Nat. Commun.* **13**, 4497 (2022).
- 39. A. Pol *et al.*, Rare earth metals are essential for methanotrophic life in volcanic mudpots. *Environ. Microbiol.* **16**, 255-264 (2014).
- 40. Y. W. Deng, S. Y. Ro, A. C. Rosenzweig, Structure and function of the lanthanide-dependent methanol dehydrogenase XoxF from the methanotroph *Methylomicrobium buryatense* 5GB1C. *J. Biol. Inorg. Chem.* **23**, 1037-1047 (2018).
- 41. G. J. P. Deblonde, A. Chagnes, G. Cote, Recent advances in the chemistry of hydrometallurgical methods. *Sep. Purif. Rev.* **52**, 221-241 (2022).
- 42. D. Stamberga *et al.*, Structure Activity Relationship Approach toward the Improved Separation of Rare-Earth Elements Using Diglycolamides. *Inorg. Chem.* **59**, 17620-17630 (2020).
- 43. T. Cheisson, B. E. Cole, B. C. Manor, P. J. Carroll, E. J. Schelter, Phosphoryl-Ligand Adducts of Rare Earth-TriNOx Complexes: Systematic Studies and Implications for Separations Chemistry. *ACS Sustain. Chem. Eng.* 7, 4993-5001 (2019).
- 44. Z. Dong, J. A. Mattocks, J. A. Seidel, J. A. Cotruvo, D. M. Park, Protein-based approach for high-purity Sc, Y, and grouped lanthanide separation. *Sep. Purif. Technol.* **333**, 125919 (2024).
- 45. G. Verma *et al.*, Investigation of Rare Earth Element Binding to a Surface-Bound Affinity Peptide Derived from EF-Hand Loop I of Lanmodulin. *ACS Appl. Mater. Interfaces* **16**, 16912-16926 (2024).
- 46. G. Bhardwaj *et al.*, Accurate de novo design of hyperstable constrained peptides. *Nature* **538**, 329-335 (2016).
- 47. H. N. Vu *et al.*, Lanthanide-dependent regulation of methanol oxidation systems in *Methylobacterium extorquens* AM1 and their contribution to methanol growth. *J. Bacteriol.* **198**, 1250-1259 (2016).
- 48. E. R. Featherston *et al.*, Biochemical and structural characterization of XoxG and XoxJ and their roles in lanthanide-dependent methanol dehydrogenase activity. *ChemBioChem* **20**, 2360-2372 (2019).
- 49. M. Wehrmann, C. Berthelot, P. Billard, J. Klebensberger, Rare earth element (REE)-dependent growth of *Pseudomonas putida* KT2440 depends on the ABC-transporter PedA1A2BC and is influenced by iron availability. *Front. Microbiol.* **10**, 2494 (2019).
- 50. P. O. Juma *et al.*, Siderophore for Lanthanide and Iron Uptake for Methylotrophy and Plant Growth Promotion in *Methylobacterium aquaticum* Strain 22A. *Front. Microbiol.* **13** (2022).
- 51. L. Gorniak, J. Bechwar, M. Westermann, F. Steiniger, C.-E. Wegner, Different lanthanide elements induce strong gene expression changes in a lanthanide-accumulating methylotroph. *Microbiol. Spectrum* 11, e00867-00823 (2023).